ELSEVIER

Journal of Quantitative Spectroscopy & Radiative Transfer 109 (2008) 1347–1362

Journal of Quantitative Spectroscopy & Radiative Transfer

www.elsevier.com/locate/jqsrt

# The spatial polarization distribution over the dome of the sky for abnormal irradiance of the atmosphere

V.P. Budak*, S.V. Korkin

*Light Engineering Department, Moscow Power Engineering Institute (TU), 111250 Moscow, Russia*

Received 12 September 2007; received in revised form 2 December 2007; accepted 16 January 2008

**Abstract**

The paper deals with the polarized radiative transfer within a slab irradiated by a collimated infinitely wide beam of arbitrary polarized light. The efficiency of the proposed analytical solution lies in the assumption that the complete vectorial radiative transfer solution is the superposition of the most anisotropic and smooth parts, computed separately. The vectorial small-angle modification of the spherical harmonics method is used to evaluate the anisotropic part, and the vectorial discrete ordinates method is used to obtain the smooth one. The azimuthal expansion is used in order to describe the light field spatial distribution for the case of abnormal irradiance and to obtain some known neutral points in the sky especially useful for polarized remote sensing of the atmosphere.


*Keywords:* Polarized radiative transfer; Complete solution

## 1. Introduction

It is well known in optics that polarization state of light described by four-element Stokes vector (SV) contains all the information about an object under consideration available for optical methods of remote sensing (RS). Nevertheless today the number of scalar (neglecting polarization) studies is much more than polarimetric ones. This relates with the comparatively small number of polarimetric systems all over the world. And this fact in turn can be explained by two main reasons: design problems in electro-optical polarimetric systems (high accuracy of measurements must be applied to determine the polarization state of light) and mainly by absence of a reliable mathematical model including polarization for interpretation of the experimental results (see Polarization Science and Remote Sensing II, SPIE 5888 (2005), for example—quite many polarimetric systems and simultaneously only a few theoretical investigations). Following the scalar case the polarized radiative transfer (RT) mathematical model must be of high efficiency from the point of view of the numerical solutions's convergence to the exact one. It must allow to compute highly anisotropic scattering of natural formations (clouds, ocean, galaxy dust and others) and must be valid for arbitrary optical thickness $\tau$ and the irradiance angle $\theta_o$ of a scattering media (the last one allows to describe known directions of neutral

*Corresponding author. Tel.: +7 495 362 7067; fax: +7 495 362 7494.
*E-mail address:* budakvp@mpei.ru (V.P. Budak).

0022-4073/$ - see front matter © 2008 Elsevier Ltd. All rights reserved.
doi:10.1016/j.jqsrt.2008.01.014

polarization of atmosphere-scattered light—Arago, Babinet and Brewster points). The model must include multiple scattering and if possible the solution must be expressed in analytical form to make the evaluation of inverse problems a little simpler. This paper deals with a described model applied to a slab irradiated by infinitely wide collimated beam (plain unidirectional (PU) source of radiation with $\hat{\mathbf{l}}_0$ as a direction of the irradiation). The incident light is assumed to be both natural and arbitrary polarized in different calculated examples.

## 2. The anisotropic part

The approach described here is considered in Ref. [1] both for vectorial but mainly for 3D scalar approximation together with main references. Here we concentrate on the vectorial case more deeply. We will use the following notation: "$\rightarrow$" is the four-element column vector; "$\leftrightarrow$" is the 16-element square Mueller matrix; $\Lambda$ is the single scattering albedo; $\theta$ and $\varphi$ are zenithal and azimuthal angles respectively; $\mu = \cos\theta$, the unit directionality vector is $\hat{\mathbf{l}}$. The SV and its component we note as $\vec{L} = [I \quad Q \quad U \quad V]^{\mathrm{T}}$, "T" is the transpose operation. In RT one of the main problems is to take mathematical features of the boundary problem for the vectorial radiative transfer equation (VRTE) into account. These features are caused by ray approximation of radiation's propagation description. For the PU-source such mathematical feature is the non-scattered radiation expressed as Dirac δ-singularity. This singularity needs infinite number of elements to be represented in a series and hence cannot be computed analytically. Chandrasekhar separated the light field within the slab into two parts—δ-singularity and scattered light—and computed the diffuse transparent and reflected light field [2]. But for real turbid media, the scattered light field still remains a highly anisotropic function which needs lots of terms of the series to be computed. This leads to the ill-conditionality of the evaluations and besides computation time increases.

We follow with an idea that showed good results for the scalar case [3–6] and represent the desired vectorial radiation field as the superposition of the anisotropic part that includes the δ-singularity and smooth non-small angle part (indexed by "R"—regular part). So we write for the desired spatial distribution of SV (see Fig. 1) the following equation:

$$\vec{L}(\tau, \hat{\mathbf{l}}) = \vec{L}_{\mathrm{R}}(\tau, \hat{\mathbf{l}}) + \vec{L}_{\mathrm{SA}}(\tau, \hat{\mathbf{l}}). \tag{1}$$

We use the definition, the addition theorem and some recurrence formulas from Gelfand [7] for generalized spherical functions (GSF)

$$\overleftrightarrow{Y}^k_m(\mu) = \mathrm{Diag}[P^k_{m,+2}(\mu);\ P^k_{m,+0}(\mu);\ P^k_{m,-0}(\mu);\ P^k_{m,-2}(\mu)],$$

which represent the eigenfunctions for the scattering operator of the VRTE and write down the standard series to express SV and the scattering matrix $\overleftrightarrow{x}$ as follows (both in circular polarization [8]—CP, usually used in polarized radiative transfer problems):

$$\vec{L}_{\mathrm{CP}}(\tau, \hat{\mathbf{l}}) = \sum_{m=-\infty}^{\infty} \sum_{k=0}^{\infty} \frac{2k+1}{4\pi} \overleftrightarrow{Y}^k_m(\mu) \vec{f}^k_m(\tau) \exp(im\varphi),$$

$$[\overleftrightarrow{x}(\hat{\mathbf{l}}\hat{\mathbf{l}}')]_{r,s} = \sum_{k=0}^{\infty} (2k+1) x^k_{r,s}(\tau) P^k_{r,s}(\hat{\mathbf{l}}\hat{\mathbf{l}}'). \tag{2}$$

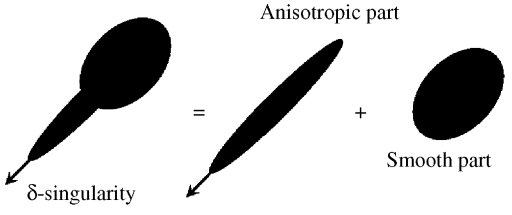


Fig. 1. The superposition of two parts—anisotropic (containing all singularities) and smooth one—schematically.

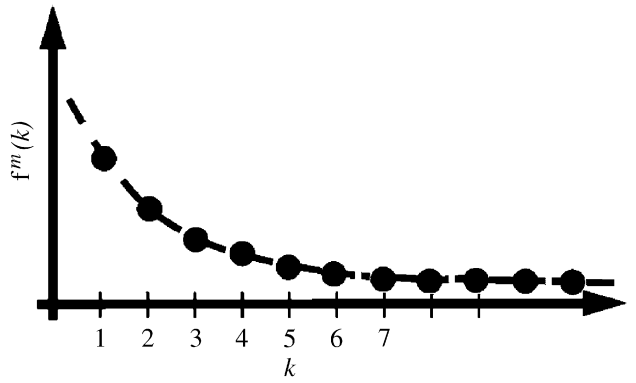


Fig. 2. The spatial spectrum is approximated by a continuous function with respect to discrete general spherical function's order $k$.

The anisotropic part is computed in the vectorial small-angle modification of the spherical harmonics method (VMSH) [9]. The VMSH (as well as the MSH itself—the scalar form of the VMSH) is built upon the substitution of the discrete spatial spectrum of the SV $\vec{f}_k^m$ in Eq. (2) with respect to zenithal index $k$ by a smooth $k$-continuous one as it is shown on Fig. 2 (the smoothness is certainly the assumption):

$$\vec{f}^m(\tau, k \pm 1) \approx \vec{f}^m(\tau, k) \pm \frac{\partial \vec{f}^m(\tau, k)}{\partial k}. \tag{3}$$

We cut its Taylor expansion with respect to $k$ to two terms. This gives quite simple differential equation for the VMSH. The solution expresses as matrix exponent. So the VMSH can be evaluated as

$$\vec{L}_{\mathrm{VMSH}}(\tau, \hat{\mathbf{l}}, \hat{\mathbf{l}}_0) = \frac{1}{4\pi} \sum_{m=-2}^{0,2} \sum_{k=0}^{\infty} (2k+1) \overleftrightarrow{P}_k^m(\hat{\mathbf{l}}\hat{\mathbf{l}}_0) \exp\left[-(\overleftrightarrow{1} - \Lambda \overleftrightarrow{x}_k)\frac{\tau}{\mu_0}\right] \vec{f}_k^m(0) \exp\frac{im\varphi}{4\pi}, \tag{4}$$

where $\overleftrightarrow{T}_{\mathrm{SC}}$ transforms the CP-basis to Stokes polarization (SP) one, the following polynomials similar to those in Ref. [10] are used: $R_m^k(\mu) = 0.5[P_{m,2}^k(\mu) + P_{m,-2}^k(\mu)]$, $T_m^k(\mu) = 0.5[P_{m,2}^k(\mu) - P_{m,-2}^k(\mu)]$. And the matrix polynomials are

$$\overleftrightarrow{T}_{\mathrm{SC}} \overleftrightarrow{Y}_k^m(\mu) \overleftrightarrow{T}_{\mathrm{SC}}^{-1} = \overleftrightarrow{P}_k^m(\mu) = \begin{bmatrix} P_{m,0}^k(\mu) & 0 & 0 & 0 \\ 0 & R_m^k(\mu) & -\mathrm{i}T_m^k(\mu) & 0 \\ 0 & \mathrm{i}T_m^k(\mu) & R_m^k(\mu) & 0 \\ 0 & 0 & 0 & P_{m,0}^k(\mu) \end{bmatrix}.$$

All $\vec{f}_k^m(0)$ in Eq. (4) are known from boundary conditions [9]. The VMSH (4) allows evaluating the light field for some solid angle of the forward hemisphere (codirectionally with the incident radiation). This zone of validity depends greatly upon the slab properties. The more is the anisotropy state of the slab scattering properties, the wider is the zone of accurate result. Here we note that the main advantage of Eq. (4) is its keeping both the anisotropic part of light field and the direct non-scattered singularity. Approximation (4) neglects the back-scattered radiation and so we are going to describe the determination of the smooth regular part in Section 3.

## 3. Some results obtained with the VMSH

In this section we give some results for the VMSH (4) alone. We note here that the VMSH form is used to compute $\vec{L}_{\mathrm{VMSH}}(\tau, \hat{\mathbf{l}})$ in Eq. (1) and the same form will be used later in this paper to obtain the source function for the regular part $\vec{L}_{\mathrm{R}}(\tau, \hat{\mathbf{l}})$. All calculation parameters are given under the corresponding figures. The notation of the used calculation parameters, given in the figure captions, is the same as we use above. The four-element vector is the initial SV $\vec{L}_0$ illuminating the slab. The verification of the VMSH and the

discovering of the VMSH's features is produced by means of the comparison with some other methods marked as follows: MC—The Monte Carlo simulation modified by the local estimation calculation algorithm and including polarization (we give the MC-results as an error bar showing the dispersion of the numerical result in the corresponding points); SS is the single scattering approximation method including polarization; SHM, DOM are the scalar spherical harmonics and discrete ordinates methods, respectively. We use the well-known algorithms of the scalar RT in order to verify the first component of the SV, i.e. the total intensity of the light beam $I$. The Henyey–Greenstein matrix is used for the presented results [11] with maximum values of a linear polarization degree $P_m$ and an ellipticity $Q_m$ within a single scattering act.

Fig. 3 shows the angle dependence of the transmitted radiation's total intensity $I(\theta)$. In spite of the fact that the phase function anisotropy is not very high (Henyey–Greenstein's parameter $g = 0.5$ was assumed for this calculation) the proposed method for only anisotropy part evaluation gives good agreement with the scalar methods. The validation area spreads to the interval approximately $\pm 20^\circ$ regarding to the zenith of irradiation $\theta_o = 27^\circ$. This fact is caused as we have already mentioned by the significant anisotropy of the TOA's boundary condition. And for this example $\pm 20^\circ$ are the "small angles" ("the small-angle approximation" is only a name but not a physical meaning). The incident light is assumed to be completely linear polarized [1; 1; 0; 0]. The proposed VMSH method (solid line) is compared with solution in scalar case (spherical harmonics (SHM) and discrete ordinates (DOM) methods—the results coincide with each other). Slab parameters are $\tau = 2$, $g = 0.5$, $P_m = 0.5$, $Q_m = 0.2$, $\Lambda = 0.8$. The second feature of the VMSH can be seen clearly from the presented figure: the trimming of the Taylor series to two terms (3) gives the neglecting of the back-scattered radiation. The neglecting of the scattering photon trajectories' dispersion itself gives the forthcoming erroneous results for the backscattered radiation. Particularly the bottom boundary conditions and the radiation reflected by the slab cannot be included in the VMSH. In an effort to eliminate all these defects, i.e. to include the bottom boundary conditions, to calculate the reflected radiation and finally to build a mathematical model of the polarized radiative transfer suitable for polarized satellite RS of the aerosol formations, the regular part of the complete VRTE solution will be evaluated in this paper a little later.

And finally we would like to note one more feature in accordance with the figure under consideration: the initial radiation is fully linear polarized [1, 1, 0, 0]. The scalar methods neglect the polarization state of the

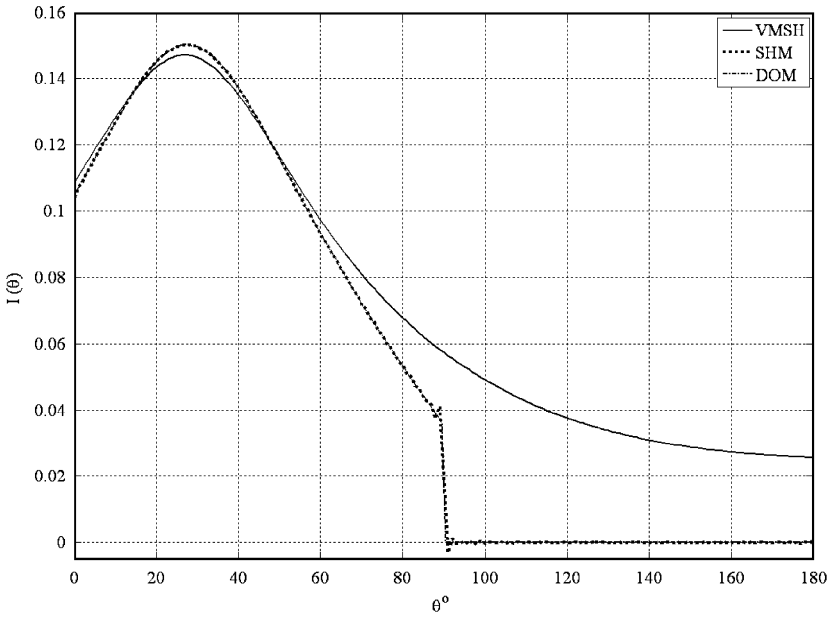


Fig. 3. The total intensity $I(\theta)$ zenith dependence for Henyey–Greenstein scattering with average scattering $\cos g = 0.5$, scattering matrix parameters $P_m = 0.5$, $Q_m = 0.2$, angle of irradiation $\theta_o = 27^\circ$, single scattering albedo $\Lambda = 0.8$, optical depth $\tau = 2$. The Stokes vector for the incident light is $\vec{L}_0 = [1 \quad 1 \quad 0 \quad 0]^T$. The proposed method VMSH (solid line) is compared with scalar spherical harmonics (dot) and discrete ordinates (dash-dot) methods.

incident radiation of course and consider only the total intensity of the radiation. But in spite of this fact we did not notice any significant error for the cases of scalar and polarized RT when only the *I*-component is considered (in this calculation and in many others). So if only the total intensity is needed in the considered examples the scalar methods will suite the researcher.

Fig. 4 shows the polarization degree's zenith distribution for quite smooth Rayleigh scattering matrix. As shown in Fig. 4 a smooth scattering is present but in spite of this the agreement is good because of the boundary problem's singularity. The VMSH describes some known facts for Rayleigh scattering: the greater is the scattering angle (to be exact the zenith angle of observation), the higher is the polarization state of the scattered radiation. The radiation scattered forward for the normal irradiance is unpolarized and the polarization degree's culmination for the Rayleigh scattering is 90°. An insignificant deviation of the VMSH and the SS occurred together with the sight angle increase caused by increase of the optical thickness for the inclined directions (the greater the inclination, the higher is the deviation). The proposed method VMSH (solid line) is compared with the Monte Carlo simulation (MC—error bar) modified by local estimation algorithm and single scattering (SS—dot line) approximation. Slab parameters are $\tau = 1$, $\Lambda = 0.2$. The incident light is natural and the irradiance angle is normal.

As one can see from Fig. 5, the small-angle area depends greatly upon the calculation conditions. Total intensity $I(\theta)$ dependence is shown. Contrary to Fig. 1 a quite sharp scattering is assumed: $g = 0.95$ and for the phase function anisotropy degree we can write $x(0^\circ)/x(180^\circ) = (1+g)^2/(1-g)^2 \approx 1500$. It is evident from the figure that the whole forward hemisphere $\theta \in [0^\circ \cdots 90^\circ]$ is the validation area for the VMSH. So we conclude that the scattering anisotropy or smoothness influences mostly on the width of the field of the VMSH application. And meanwhile the "small-angle" area of the VMSH's correctness presents the independence on the scattering anisotropy degree (if the optical depth $\tau$ is not large of course: the higher the anisotropy of the scattering, the greater can be the optical depth for the VMSH validity). The incident light is assumed to be completely unpolarized, and the incident angle is $\theta_o = 40^\circ$. The proposed VMSH method (solid line) is compared with solution in scalar case (spherical harmonics (SHM) and discrete ordinates (DOM) methods—the results coincide with each other) and the Monte Carlo simulation modified by local estimation.

Fig. 6 demonstrates the known Umov's law: the greater are the conservation properties of the slab (i.e. the greater is the survival probability of the photon during the interaction with a particle of the slab—the

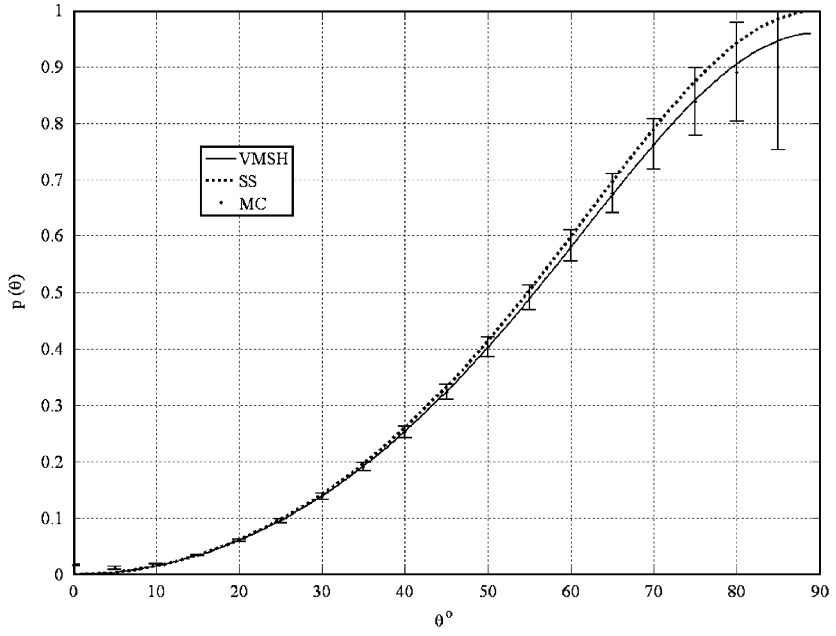


Fig. 4. The polarization degree $p(\theta)$ dependence for Rayleigh scattering. Slab parameters are $\tau = 1$, $\Lambda = 0.2$. The VMSH is compared with single scattering approximation (dot) and Monte Carlo simulation (error bar).

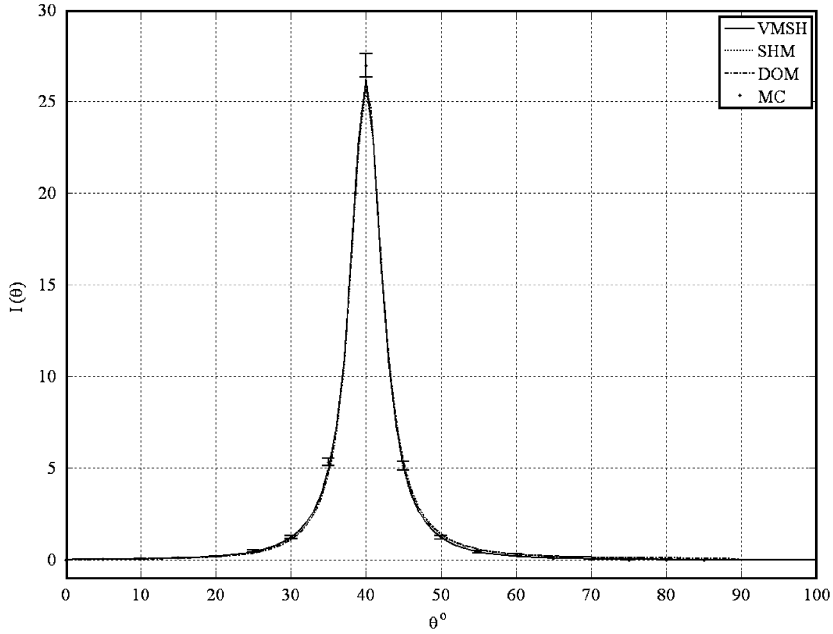


Fig. 5. The total intensity $I(\theta)$ zenith dependence for Henyey–Greenstein scattering with average scattering $\cos g = 0.95$, scattering matrix parameters $P_m = 0$, $Q_m = 0$, angle of irradiation $\theta_o = 40^\circ$, single scattering albedo $\Lambda = 0.99$, optical depth $\tau = 1$. The Stokes vector for the incident light is $\vec{L}_0 = [1 \quad 0 \quad 0 \quad 0]^T$. The proposed method VMSH (solid line) is compared with scalar spherical harmonics (dot) and discrete ordinates (dash-dot) methods and polarized Monte Carlo simulation (error bar).

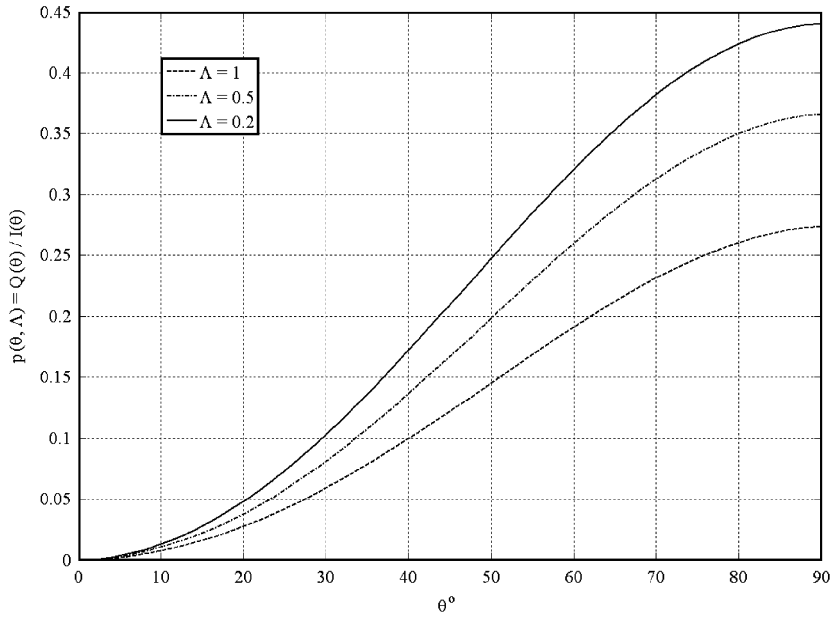


Fig. 6. The polarization degree $p(\theta, \Lambda)$ zenith dependence for Henyey–Greenstein scattering with average scattering $\cos g = 0.9$, $P_m = 0.5$ and $Q_m = 0.2$, normal irradiation by a non-polarized beam, and $\tau = 5$.

scattering albedo $\Lambda$), the weaker is the degree of polarization of this radiation. The polarization degree $p(\theta, \Lambda)$ dependence for the proposed method VMSH and different $\Lambda$ is shown. The incident light is natural and the irradiance angle is normal. Further on we give four figures in order to demonstrate the features of the VMSH.

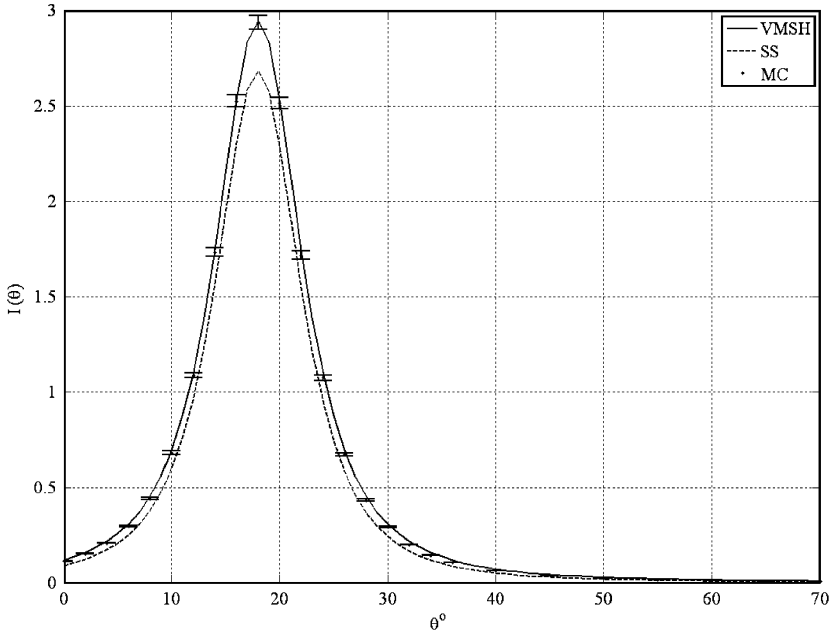


Fig. 7. The first Stokes vector component $I(\theta)$ dependence. The slab thickness $\tau_0 = 0.5$, the albedo $\Lambda = 0.6$ the anisotropy is defined by $g = 0.9$. The Henyey–Greenstein scattering matrix parameters are $P_m = 0.5$ and $Q_m = 0.2$, the irradiation angle is $\theta_o = 18^\circ$ and the initial Stokes vector is assumed to be both partially linear and elliptically polarized [1; 0.7; 0; −0.5]. The result is compared with single scattering approximation and Monte Carlo simulation.

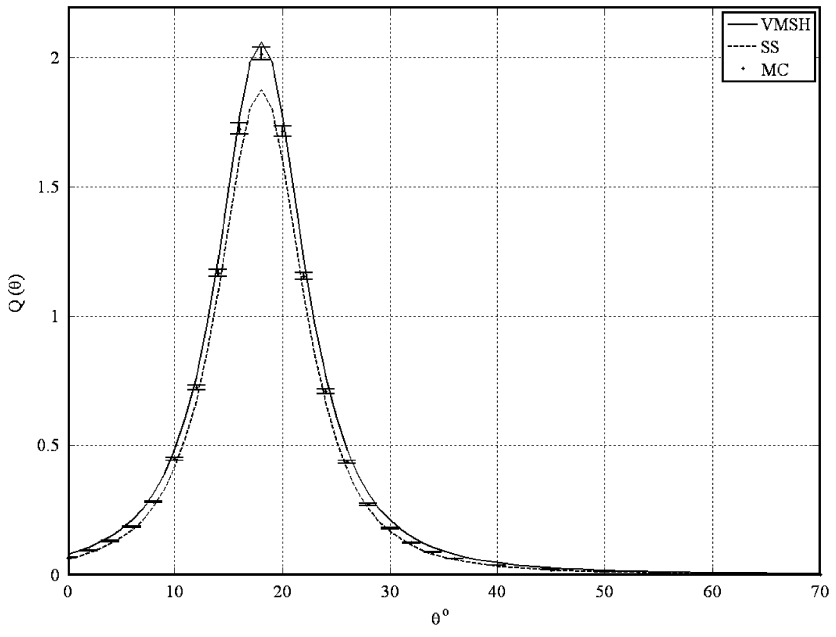


Fig. 8. The second Stokes vector component $Q(\theta)$ zenith dependence for the calculation parameters of Fig. 7.

The calculation parameters are identical for all these figures. We assume the slab thickness $\tau_0$ to be 0.5, the albedo $\Lambda$ is 0.6 the anisotropy is defined by $g = 0.9$. The Henyey–Greenstein scattering matrix parameters are $P_m = 0.5$ and $Q_m = 0.2$ (i.e. not only the linear polarization but the ellipticity generation while scattering is assumed as well). The slab is irradiated with the direction $\theta_o = 18^\circ$ and the initial SV is assumed to be both

partially linear and elliptically polarized—[1; 0.7; 0; −0.5]. We give all four components of the SV within the slab for the forward hemisphere together with MC- and SS-calculations. We specially note that the calculated dispersion for the MC calculations of the $U$-component (it is absent in the incident radiation and is generated only while multiple scattering within the slab) turned out to be enormous compared with the value of $U$-component even for thousands of trajectories. That is why the MC calculation is absent in Fig. 9. And the fact that for Figs. 7–10 the modulo of the SS is smaller compared with the according VMSH cases we explain

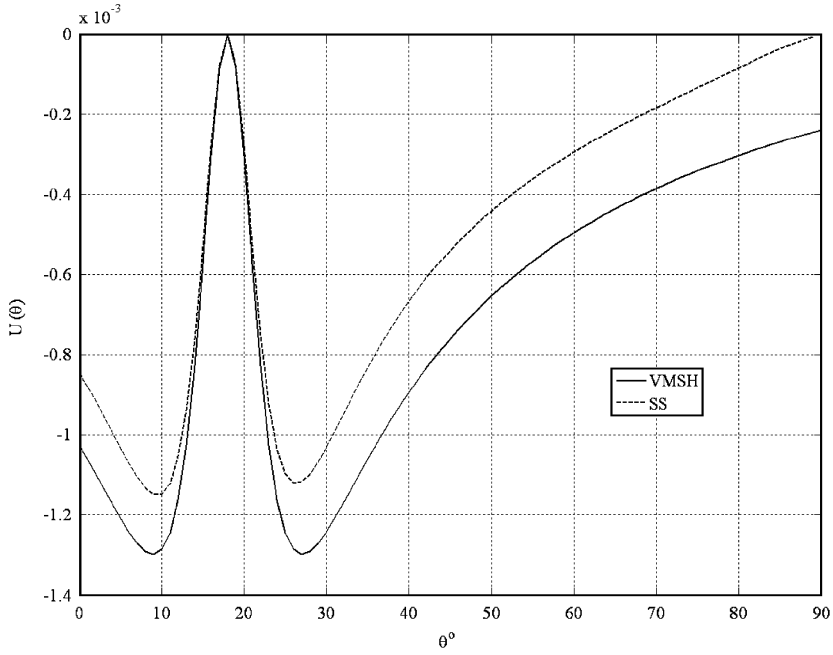


Fig. 9. The third Stokes vector component $U(\theta)$ zenith dependence for the calculation parameters of Fig. 7.

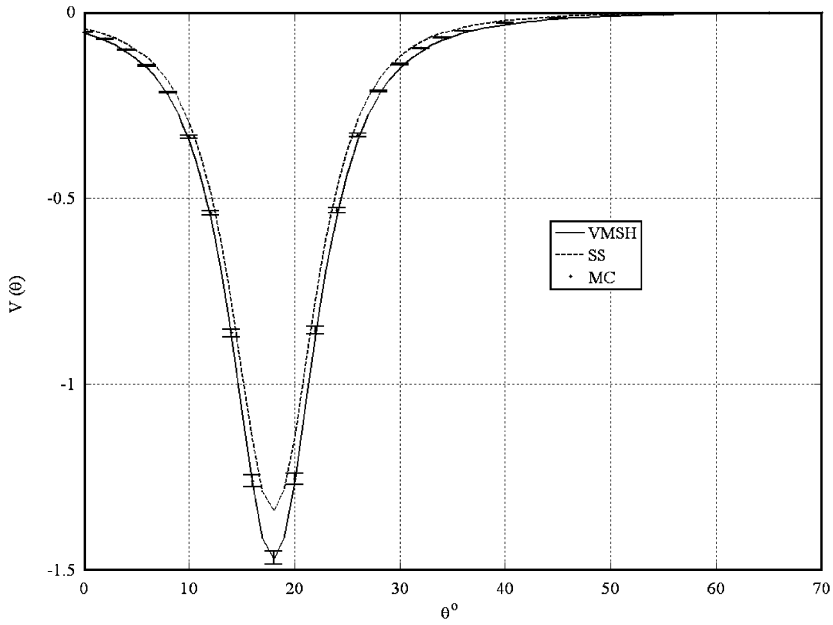


Fig. 10. The fourth Stokes vector component $V(\theta)$ zenith dependence for the calculation parameters of Fig. 7.

by the fact that the VMSH includes multiple scattering and the slab is not thin enough for only one scattering act for each photon takes place (note that MC coincides quite well with the VMSH everywhere except $U$-component).

## 4. The smooth part

As we noted above we depart from Chandrasekhar and formulate the boundary problem not for the whole diffuse radiation but for the smooth part only as follows:

$$\begin{cases} \mu\frac{\partial}{\partial\tau}\vec{L}_{\mathrm{R}}(\tau,\hat{\mathbf{l}})+\vec{L}_{\mathrm{R}}(\tau,\hat{\mathbf{l}})=\frac{\Lambda}{4\pi}\oint\overleftrightarrow{R}(\hat{\mathbf{l}}\times\hat{\mathbf{l}}'\to\hat{\mathbf{z}}\times\hat{\mathbf{l}})\overleftrightarrow{x}(\hat{\mathbf{l}}\hat{\mathbf{l}}')\overleftrightarrow{R}(\hat{\mathbf{z}}\times\hat{\mathbf{l}}\to\hat{\mathbf{l}}\times\hat{\mathbf{l}}')\vec{L}_{\mathrm{R}}(\tau,\hat{\mathbf{l}}')\,\mathrm{d}\hat{\mathbf{l}}'+\vec{\Delta}(\tau,\hat{\mathbf{l}}),\\ \vec{L}(0,\hat{\mathbf{l}})|_{\mu>0}=\vec{0};\quad \vec{L}(\tau_0,\hat{\mathbf{l}})|_{\mu<0}=-\vec{L}_{\mathrm{VMSH}}(\tau_0,\hat{\mathbf{l}}). \end{cases} \tag{5}$$

The VMSH as the source function is described by $\vec{\Delta}(\tau,\hat{\mathbf{l}})$ and can be expressed as follows:

$$\begin{aligned}\vec{\Delta}(\tau,\hat{\mathbf{l}})=&-\mu\frac{\partial}{\partial\tau}\vec{L}_{\mathrm{VMSH}}(\tau,\hat{\mathbf{l}},\hat{\mathbf{l}}_0)+\vec{L}_{\mathrm{VMSH}}(\tau,\hat{\mathbf{l}},\hat{\mathbf{l}}_0)+\frac{\Lambda}{4\pi}\oint\overleftrightarrow{R}(\hat{\mathbf{l}}\times\hat{\mathbf{l}}'\to\hat{\mathbf{z}}\times\hat{\mathbf{l}})\\ &\times\overleftrightarrow{x}(\hat{\mathbf{l}}\hat{\mathbf{l}}')\overleftrightarrow{R}(\hat{\mathbf{z}}\times\hat{\mathbf{l}}\to\hat{\mathbf{l}}\times\hat{\mathbf{l}}')\vec{L}_{\mathrm{VMSH}}(\tau,\hat{\mathbf{l}}')\,\mathrm{d}\hat{\mathbf{l}}'.\end{aligned} \tag{6}$$

Both in scalar and vectorial theories, the evaluation of scattering integral of the transport equation is at par with the δ-singularity subtraction. In vectorial case the complex circular basis (CP-representation) was offered in Ref. [8]. The matrix relation between the CP- and SP-representations is well known. The advantage point of CP is in the fact that the rotator $R^{\leftrightarrow}$ on this basis becomes a diagonal matrix and the scattering integral can be evaluated (we used this to obtain Eq. (4)). But it is impossible to use matrix scaling transformation [12] for complex numbers in order to prevent ill-conditionality of the system of equations while $\tau$ or anisotropy increases. So after evaluating of the scattering integral we transform the obtained system for $\vec{f}_k^m(\tau)$ (2) from complex CP-back to real energetic SP-basis. And for the smooth part (1) we do the same. The vectorial discrete ordinates method with Mark's boundary condition is used because of its computation efficiency. In Ref. [10] Chandrasekhar's δ-singularity subtraction was used to obtain the diffuse radiation so it is convenient to use some notations from Ref. [10] in our method of solution. As we have previously mentioned, we use the CP-representation, the GSF addition theorem and back CP→SP transformation to evaluate scattering integrals both in Eqs. (1) and (2). Besides we note that the frame of reference for Eq. (4) differs from that in Eq. (5). So we use the linear transformation to reduce the mentioned equations to the same frame of reference. Here we omit intermediate and complicated evaluations and give the main results. For the scattering integral in Eq. (5) we have

$$\vec{I}_{\mathrm{S}}=\frac{\Lambda}{2}\sum_{k=0}^{\infty}(2k+1)\sum_{m=0}^{k}\left[\overleftrightarrow{\phi}_1(m\varphi)\int_{-1}^{1}\overleftrightarrow{A}_k^m(\mu,\mu')\tilde{L}_1^m(\tau,\mu')\,\mathrm{d}\mu'+\overleftrightarrow{\phi}_2(m\varphi)\int_{-1}^{1}\overleftrightarrow{A}_k^m(\mu,\mu')\tilde{L}_2^m(\tau,\mu')\,\mathrm{d}\mu'\right], \tag{7}$$

where $\overleftrightarrow{\phi}_1(\varphi)=\mathrm{diag}\{\cos\varphi,\cos\varphi,\sin\varphi,\sin\varphi\}$; $\overleftrightarrow{\phi}_2(\varphi)=\mathrm{diag}\{-\sin\varphi,-\sin\varphi,\cos\varphi,\cos\varphi\}$, $\overleftrightarrow{x}_k$ are the matrix coefficients of scattering matrix (2) in SP-representation and $\overleftrightarrow{A}_k^m(\mu,\mu')=\overleftrightarrow{P}_k^m(\mu)\overleftrightarrow{x}_k\overleftrightarrow{P}_k^m(\mu')$. It is convenient to present the smooth part as two azimuth-dependent items

$$\vec{L}(\tau,\mu,\varphi)=\sum_{m=0}^{\infty}[\overleftrightarrow{\phi}_1(m\varphi)\overleftrightarrow{L}_1^m(\tau,\mu)+\overleftrightarrow{\phi}_2(m\varphi)\vec{L}_2^m(\tau,\mu)],$$

each of which can be obtained from the following boundary-condition problem ($i=1$ and 2) similar to Eq. (5):

$$\begin{cases}\mu\frac{\partial}{\partial\tau}\tilde{L}_i^m(\tau,\mu)+\tilde{L}_i^m(\tau,\mu)=\frac{\Lambda}{2}\sum_{k=0}^{\infty}(2k+1)\int_{-1}^{1}\overleftrightarrow{A}_k^m(\mu,\mu')\tilde{L}_i^m(\tau,\mu')\,\mathrm{d}\mu'+\Delta_i(\tau,\mu),\\ \tilde{L}_i^m(0,\mu)|_{\mu>0}=\vec{0};\quad \tilde{L}_i^m(\tau_0,\mu)|_{\mu<0}=-\vec{L}_{\mathrm{VMSH}}^m(\tau_0,\mu)|_{\mu<0},\end{cases} \tag{8}$$

if the source function $\vec{\Delta}(\tau,\hat{\mathbf{l}})$ is derived. For the source function after reduction of frames of reference, we use the same methods as described above: the SP→CP→SP transformation, the addition theorem for the GSF to

evaluate the scattering integral in Eq. (6) and the recurrence formulas for the GSF to obtain the system of equations for the vectorial coefficients. As a result we have the following for the source function

$$\vec{A}(\tau,\hat{\mathbf{l}},\hat{\mathbf{l}}_0)=\sum_{k=0}^{\infty}\sum_{m=-k}^{k}\frac{2k+1}{4\pi}\overleftrightarrow{P}_k^m(\mu)\overleftrightarrow{\Phi}_k(\tau)\overleftrightarrow{P}_k^m(\mu_0)\vec{L}_0\exp(im(\varphi-\varphi_0)), \tag{9}$$

where $\vec{L}_0=[1 \quad p\sin 2\varphi_0 \quad -p\cos 2\varphi_0 \quad q]^{\mathrm{T}}$ is the initial SV with the linear polarization degree $p$, the ellipticity $q$ and $\varphi_0$—gives the azimuth of the reference plane. Further on (in SP-basis)

$$\overleftrightarrow{\phi}_k(\tau)=\left\{\frac{1}{2k+1}\left[\overleftrightarrow{A}_{k+1}(\overleftrightarrow{1}-\Lambda\overleftrightarrow{x}_{k+1})\overleftrightarrow{Z}_{k+1}(\tau)\ \overleftrightarrow{a}_k+4\frac{2k+1}{k(k+1)}(\overleftrightarrow{1}-\Lambda\overleftrightarrow{x}_k)\overleftrightarrow{Z}_k(\tau)\overleftrightarrow{b}\right.\right.$$
$$\left.\left.+\overleftrightarrow{A}_k(\overleftrightarrow{1}-\Lambda\overleftrightarrow{x}_{k-1})\overleftrightarrow{Z}_{k-1}(\tau)\overleftrightarrow{a}_k\right]-(\overleftrightarrow{1}-\Lambda\overleftrightarrow{x}_k)\overleftrightarrow{Z}_k(\tau)\right\},\qquad \overleftrightarrow{Z}_k=\exp\left(-(\overleftrightarrow{1}-\Lambda\overleftrightarrow{x}_k)\tau_0/\mu_0\right),$$

and $\overleftrightarrow{a}_k=\mathrm{diag}[k \quad \sqrt{k^2-4} \quad k]$; $\overleftrightarrow{A}_k=\overleftrightarrow{a}_k/k$; $\overleftrightarrow{b}=\mathrm{diag}[0 \quad 1 \quad 1 \quad 0]$. This after being substituted in Eq. (9) together with Eq. (8), the VMSH (4) and assumption (1) give the complete solution of the VRTE boundary problem for an arbitrary irradiated slab.

## 5. The spatial polarization distribution over the dome of the sky for Mie and Henyey–Greenstein scattering

In this section we give some examples of the complete VRTE solution for different properties of scattering media. Haze L [13] model was used to simulate Mie-scattering. Figs. 11 and 12 contain the comparison of the proposed method verified by SS-approximation for a thin slab. This method of control of the results seems very efficient because of the simple analytical form of SS. Both of the discussed figures show that the polarization degree obtained by SS is higher in some areas compared with multiple scattering. This fact can be explained in a simple way: SS-model is only the approximation—all the subsequent scattering acts described by proposed method lead to a depolarization. But such cases are seldom for the selected slab's parameters—so the deviation of the results is not large. A well-known effect of non-polarized radiation's scattering exactly

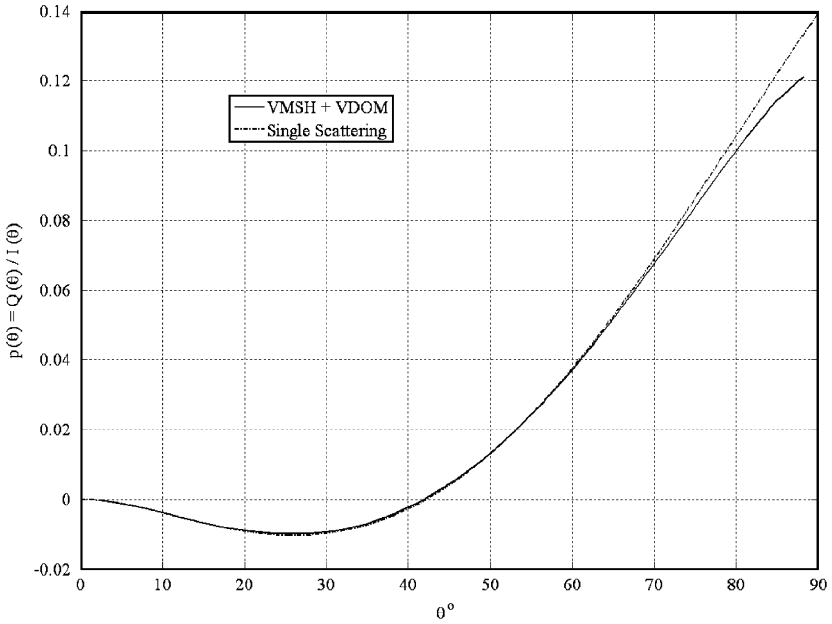


Fig. 11. The polarization degree $p(\theta)$ dependence for Mie-scattering-transmitted radiation. Slab parameters are $\tau=0.1$, $\Lambda=0.9$. The complete VRTE solution obtained by described VMSH + VDOM method (solid line) is compared with single scattering approximation (dash-dot). Normal irradiation.

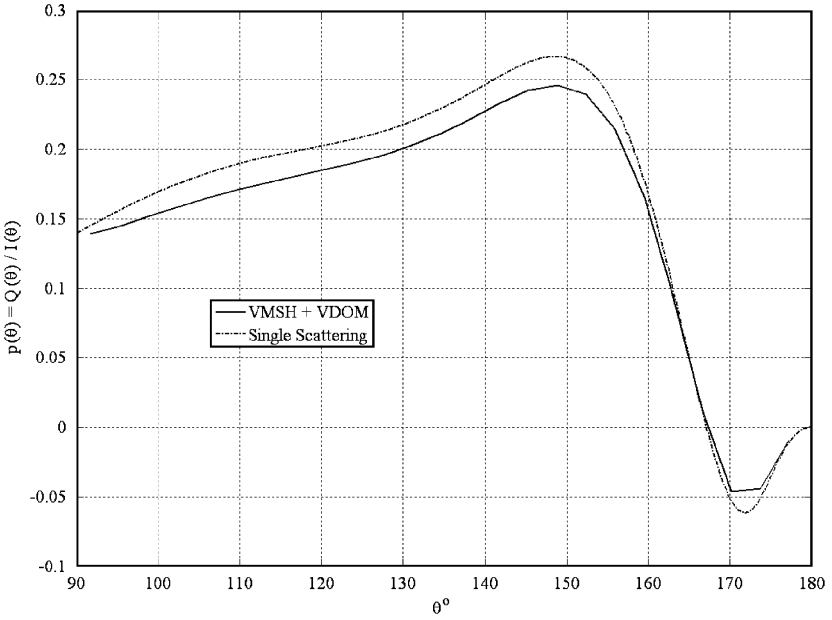


Fig. 12. The same as in Fig. 11 but for reflected radiation.

forward and backward can be seen together with neutral points both in transmitted and reflected radiation. Slab parameters are $\tau = 0.1$, $\Lambda = 0.9$.

Fig. 13 demonstrates the advantage of the described method of the complete anisotropic part subtraction compared with classic non-scattered radiation subtraction [10]. We need only $K = 40$ GSF in our method VMSH + VDOM to make the computation that needs more 150 GSF for standard computation method. The $K$-advantage increases fast together with the scattering anisotropy degree (especially for ocean scattering and particles scattering) and azimuthal expansion for abnormal irradiance increase.

Fig. 14 shows some results for Henyey–Greenstein scattering depending on the optical thickness of the slab. It can be seen that for the reflected radiation's polarization state, a critical optical depth is present. The radiation scattered deeper than this critical optical depth does not influence upon the total reflected radiation (for example such optical depths as $\tau = 50$, 100 and $\infty$ cannot be distinguished in the non-conservative case).

Figs. 15 and 16 give some more results for Mie-scattering. Some neutral points can be seen in both these figures. Both of them show the depolarization degree increasing together with the thickness of a slab. The comparison of the reflected radiation's polarization state for Mie (Fig. 16) and Henyey–Greenstein (Fig. 14) discovers that multiple scattering (optically deep slabs) makes the non-small angle features of the scattering matrix elements (''wings'' of Mie-scattering matrix elements) even. This fact in its turn leads to the following: the Henyey–Greenstein approximation formula turns out to be good enough for multiple Mie-scattering acts. That is why Fig. 16 shows almost monotonic functions for deep slabs ($\tau = 5$, 10).

Figs. 17–20 give some results for abnormal irradiance of the slab. Fig. 17 shows the second SV component $Q$ with respect to zenithal angle and for two optical thickness of the slab. We compared the result including multiple scattering (MS lines on the figure) with a single scattering (SS lines) one. One can see from the figure that for pure scattering media, MS and SS results are identical. But the difference between the results increases together with the increase of the scattering properties of the media. Hence we conclude that the SS approximation being good enough for some cases—for clear atmosphere for example—is invalid for analyzing radiative transfer in cloudy layers. Fig. 18 is the same as in Fig. 17 but for reflected radiation. The calculation parameters are $\theta_o = 30^\circ$, Henyey–Greenstein scattering with $g = 0.9$, $\Lambda = 0.8$, $P_m = 0.5$, $Q_m = 0$.

Figs. 19 and 20 give the zenithal distribution of the reflected radiation polarization degree with respect to different thickness of the slab (Fig. 19) or with respect to different single scattering albedo. The last one shows a known fact—the higher is the scattering albedo, the smaller is the polarization degree (Umov's law). And

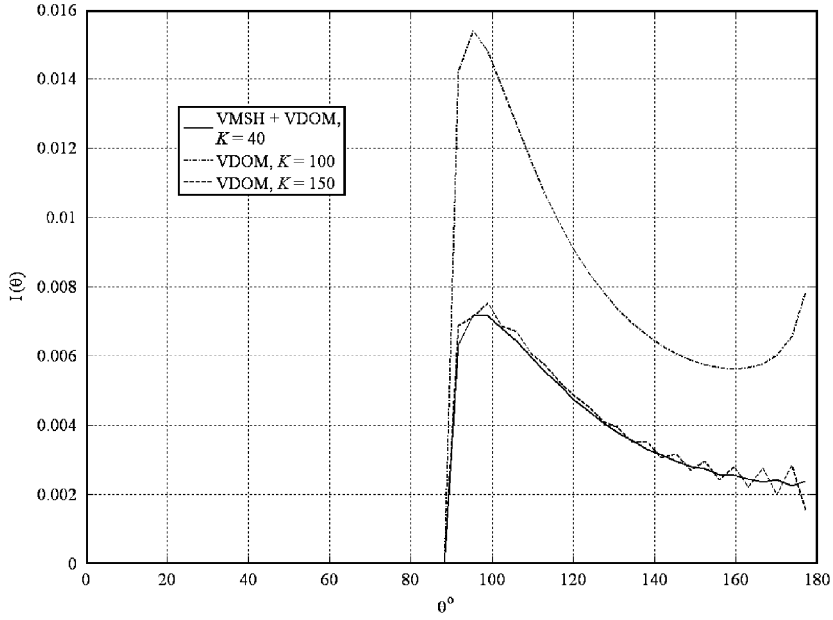


Fig. 13. The efficiency of the proposed method: we compare our method (VMSH + VDOM solid line) with $K = 40$ expansion terms with standard method of only singularity subtraction—vectorial discrete ordinates method (VDOM—dash-dot and dash lines foe different orders of approximation). More long series for standard calculation case are needed. Total intensity is shown.

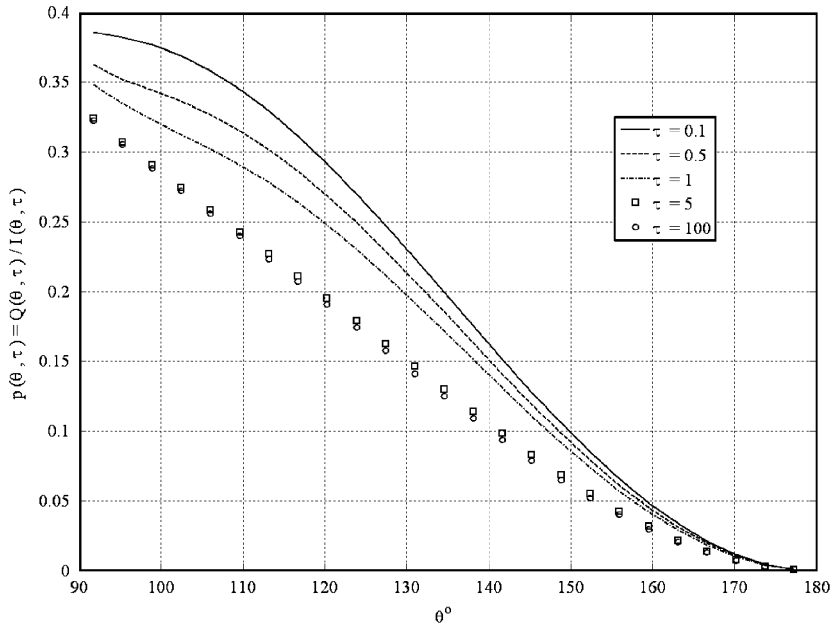


Fig. 14. The spatial dependence of the polarization state $p(\theta, \tau)$ dependence for Henyey–Greenstein scattering ($g = 0.9$, $\Lambda = 0.8$)-reflected radiation.

finally we note for Fig. 19 that there is a critical threshold for a slab's thickness. Scattering processes occurring deeper compared with this critical optical thickness do not influence the reflected polarization state because of the weakening of the SV components. The calculation parameters are $\theta_o = 40^\circ$, $g = 0.95$, $P_m = 0.5$, $Q_m = 0.2$, $\Lambda = 0.8$ for Fig. 19 and $\theta_o = 20^\circ$, $g = 0.9$, $\tau = 5$, $P_m = 0.9$, $Q_m = 0$ for Fig. 20.

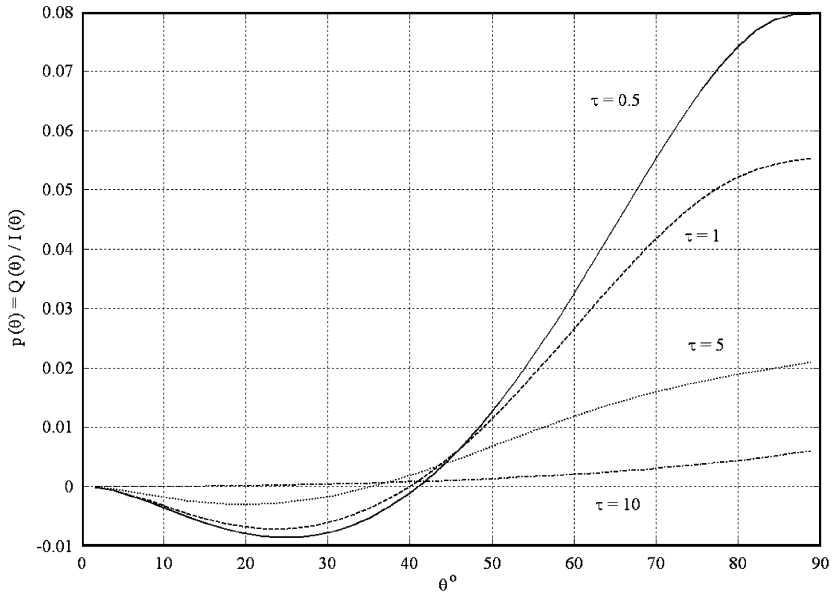


Fig. 15. The spatial dependence of the polarization state $p(\theta, \tau)$ for Mie-scattering-transmitted radiation.

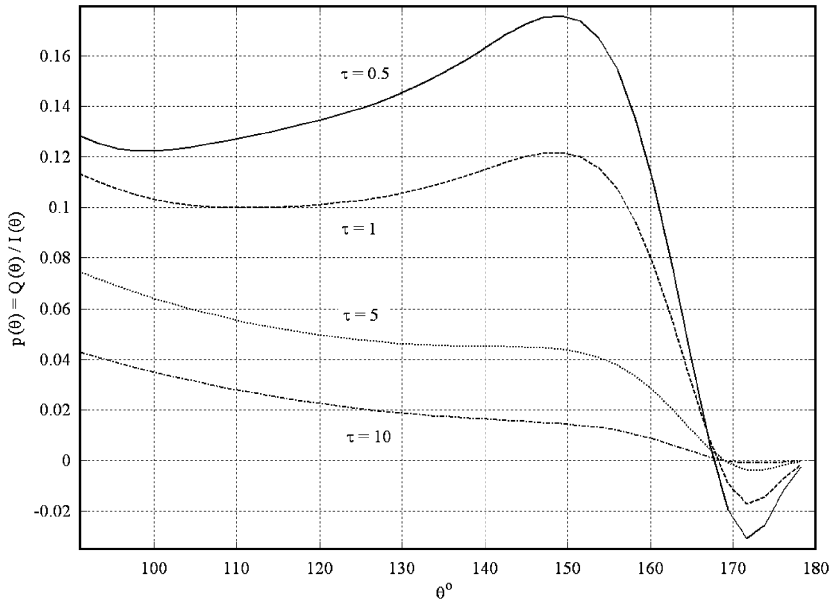


Fig. 16. The spatial dependence of the polarization state $p(\theta, \tau)$ for Mie-scattering–reflected radiation.

## 6. Conclusion

In conclusion we would like to note one thing, we have mentioned above, for the second time: δ-singularity subtraction and the subsequent determination of the scattered radiation seem to be inefficient for the cases of highly anisotropic scattering and the VRTE boundary condition's mathematical features presence. One can find such features not only for PU-source but for point-sources too. So the only way to build an efficient model for such cases is to consider the superposition of the anisotropic and regular parts. We particularly note that the efficiency of the proposed method increases together with the degree of scattering anisotropy, the

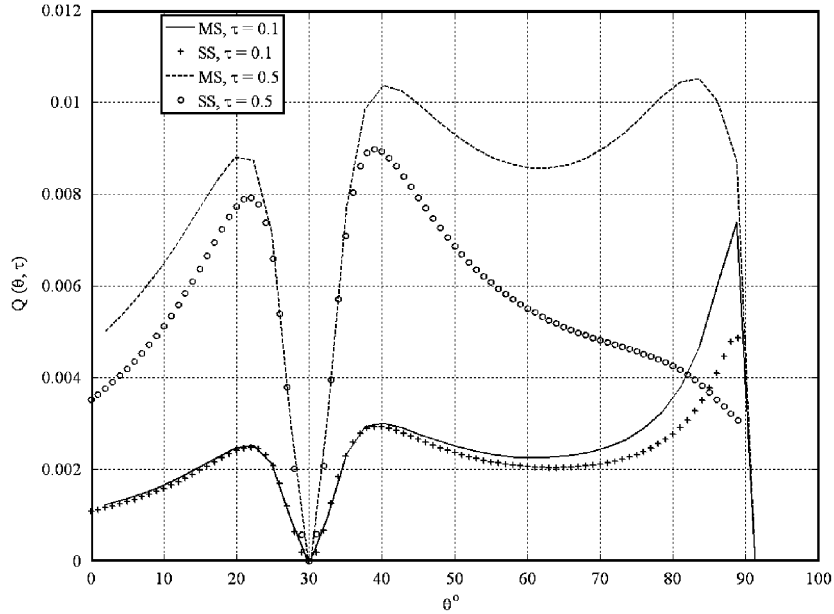


Fig. 17. The spatial dependence of the second component $Q(\theta,\tau)$ of the Stokes vector for forward hemisphere-transmitted radiation. The irradiation angle is $\theta_o = 30^\circ$, Henyey–Greenstein scattering matrix parameters are $g = 0.9$, $P_m = 0.5$, $Q_m = 0$, albedo is $\Lambda = 0.8$.

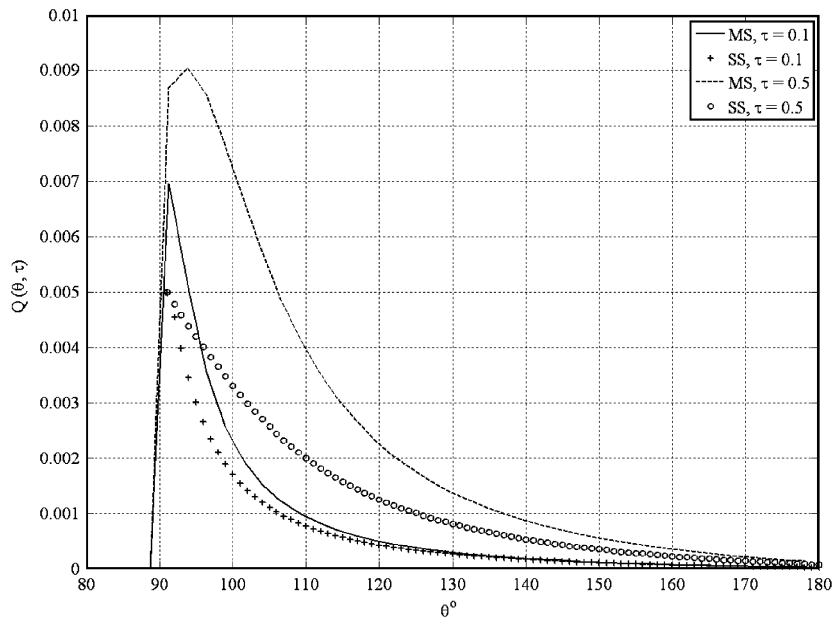


Fig. 18. The same as in Fig. 17 but for reflected radiation.

number of stratification layers of a slab (for example, four layers to simulate a real atmosphere), for 2D and 3D geometry (point-source is the simple example).

The VMSH itself is quite a complete tool to calculate the solar radiation scattered by the atmosphere aerosol and reaching the Earth. This fact is explained by high scattering anisotropy degree of atmosphere but mainly by ray approximation that describes the singularity of the VRTE solution. The efficiency of the complete VRTE solution obtained by means of the described method lies in the decomposition of the problem

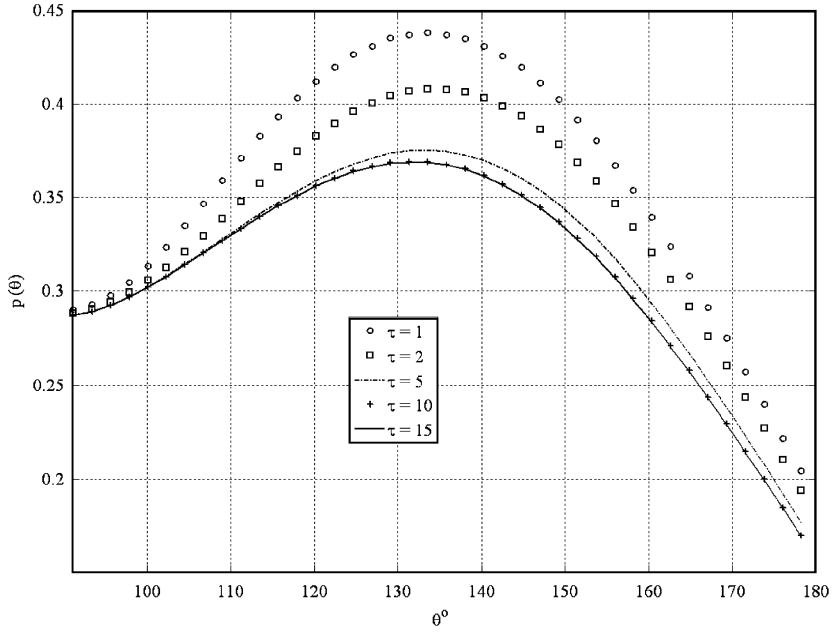


Fig. 19. Spatial dependence $p(\theta,\tau)$ for reflected radiation and abnormal incident. Henyey–Greenstein scattering matrix parameters are $g=0.95$, $P_m=0.5$, $Q_m=0.2$, natural light irradiation angle $\theta_o=40^\circ$, albedo is $\Lambda=0.8$.

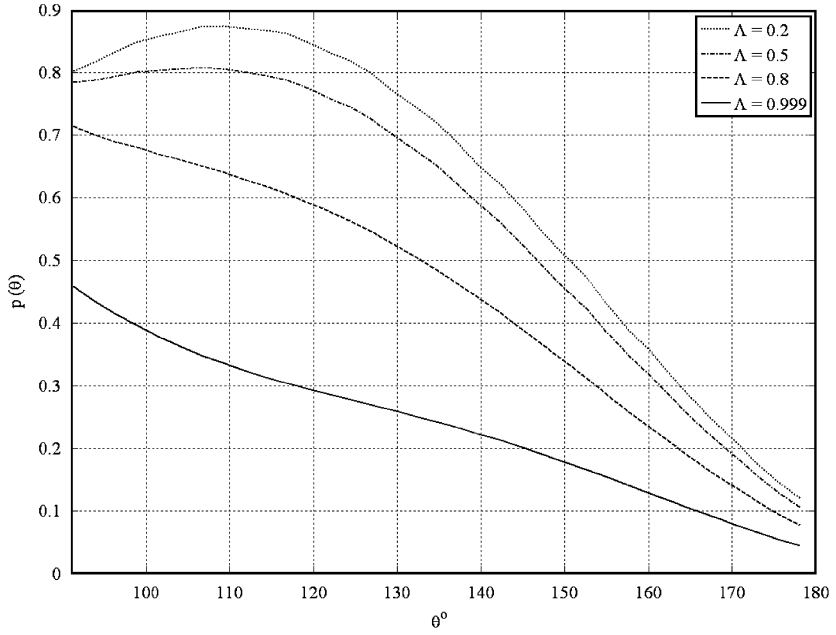


Fig. 20. Angle-dependence $p(\theta,\Lambda)$ for reflected radiation and abnormal incident. Henyey–Greenstein scattering matrix parameters are $g=0.9$, $P_m=0.9$, $Q_m=0$, natural light irradiation angle $\theta_o=20^\circ$, slab's depth $\tau=5$.

into two parts—separately for anisotropic part and smooth part. The anisotropic part is very exigent for the order of the GSF series expansion. But at the same time, the geometry of the anisotropic part leads to the described simplification of the VRTE to the VMSH form. The simplification of the VRTE together with the smoothness of the regular part determines the advantages of the VMSH + VDOM method. The

Henyey–Greenstein phase matrix is a good form for the description of the forward scattered light. Hence, it is quite convenient to be used together with the VMSH. But in the case of natural aerosol description—especially of its polarization properties applied to the complete VRTE solution for the purposes of remote sensing, the Mie theory must be used necessarily. In addition to the phase matrix form, we note that the widely used block-diagonal form of scattering matrix is incomplete in general case and additional investigation of real scattering matrix forms must be carried out.

And finally we note one feature of the polarized RT description that has not been discussed yet. Here in this paper we used a well-known CP-representation for the SV and the phase matrix. Having evaluated the scattering integral of the VRTE, we turned back to SP in order to operate with real-number energetic units and to use scaling transformation [12]. But it is not necessary to use SP–CP–SP transformation. This serial transformation leads to the form of matrix GSF described above in Eq. (4). If we let $\overleftrightarrow{P}_k^m(\mu)$ to be the basic function instead of $\overleftrightarrow{Y}_k^m(\mu)$ we will be able to omit complex-number CP-transformation (if the addition theorem, the recurrence formulas and the symmetry relations are formulated for them). This problem together with complete non-block-diagonal scattering matrix consideration and reduction to 3D-polarized problems are the subjects of our current investigation.

## Acknowledgments

The authors would like to thank the members of "The Light Field in the Turbid Medium" Seminar held in the Light Engineering Department in Moscow Power-Engineering Institute (TU).

## References

[1] Budak VP, Korkin SV. On the solution of a vectorial radiative transfer equation in an arbitrary three-dimensional turbid medium with anisotropic scattering. JQSRT 2008;109:220–34.
[2] Chandrasekhar S. Radiative transfer. New York: Dover; 1960.
[3] Budak VP, Sarmin SE. Solution of the radiation transfer equation by the method of spherical harmonics in the small-angle modification. Atmos Opt 1990;3:898–904.
[4] Boudak VP. Convergence acceleration of a spherical harmonics method for strong anisotropic scattering. In: Proceeding IRS 2004: current problems in atmospheric radiation. Deepak Publishing; 2006. p. 47–50.
[5] Budak VP, Kozelskii AV, Savitskii EN. Improvement of the spherical harmonics method convergence at strongly anisotropic scattering. Atmos Ocean Opt 2004;17:28–33.
[6] Budak VP, Kozelskii AV. Accuracy and applicability domain of the small angle approximation. Atmos Opt 2005;18:32–7.
[7] Gelfand IM, Minlos RA, Shapiro ZYa. Representations of the rotation and Lorentz groups and their applications. Oxford: Pergamon Press; 1963.
[8] Kuščer I, Ribarič M. Matrix formalism in the theory of diffusion of light. Opt Acta 1959;6:42–51.
[9] Astakhov IE, Budak VP, Lisitsin DV, Selivanov VA. Solution of the vector radiative transfer equation in the small-angle approximation of the spherical harmonics method. Atmos Opt 1994;7:398–402.
[10] Siewert CE. A discrete-ordinates solution for radiative-transfer models that include polarization effects. JQSRT 2000;64:227–54.
[11] Hovenier JW, van der Mee CVM. Testing scattering matrices: a compendium of recipes. JQSRT 1996;55:649–61.
[12] Karp AH, Greenstadt J, Fillmore JA. Radiative transfer through an arbitrary thick scattering atmosphere. JQSRT 1980;24:39–406.
[13] Deirmendjian D. Electromagnetic scattering of spherical polydispersions. New York: Elsevier Publishing Company; 1969.